TU/e EINDHOVEN UNIVERSITY OF TECHNOLOGY

Threshold ionization mass spectrometry of reactive species in remote Ar/C2H2 expanding thermal plasma

Please check the document version of this publication:

• A submitted manuscript is the version of the article upon submission and before peer-review. There can be important differences between the submitted version and the official published version of record. People interested in the research are advised to contact the author for the final version of the publication, or visit the DOI to the publisher's website.
• The final author version and the galley proof are versions of the publication after peer review.
• The final published version features the final layout of the paper including the volume, issue and page numbers.

Link to publication

Threshold ionization mass spectrometry of reactive species in remote Ar/C₂H₂ expanding thermal plasma

Jan Benedikt[a)]
Department of Applied Physics, Eindhoven University of Technology, 5600 MB Eindhoven,
The Netherlands

Sumit Agarwal
Department of Chemical Engineering, University of Massachusetts, Amherst, Massachusetts 01003

Dimitri Eijkman, Wouter Vandamme, Mariadriana Creatore, and M. C. M. van de Sanden[b)]
Department of Applied Physics, Eindhoven University of Technology, 5600 MB Eindhoven,
The Netherlands

Triple stage threshold ionization mass spectrometry is successfully implemented in an Ar/C₂H₂ expanding thermal plasma setup. More than 20 hydrocarbon radicals and molecules formed in the plasma, including for example the C₂H, C₃, C₃H, and C₃H₂ radicals or C₃H₄ or C₄H₂ molecules, are measured and their absolute densities are determined. Thanks to a careful design, a high sensitivity of the instrument is achieved and species with densities as low as 1×10^{16} m^{-3} can be detected. Issues related to the absolute density calibration procedure are considered. The proper determination of the background signal by means of a beam chopper and the influence of the chopper on the measurement are discussed and the possible composition distortion of the sampled beam due to the collisions in the sampling orifice is checked. Furthermore, reported values of electron impact ionization cross sections of hydrocarbon species are compared and, based on their similarity in the near threshold energy region, the C₂H₂ electron impact ionization cross section is proposed as a reasonable approximation for other hydrocarbon radicals. The results for C, CH, and C₂ radicals are compared with previous cavity ringdown absorption spectroscopy measurements and a good agreement is obtained. © *2005 American Vacuum Society.* [DOI: 10.1116/1.2006138]

I. INTRODUCTION

Threshold ionization mass spectrometry (TIMS) is a valuable technique for characterization of vacuum-based processes.[1–4] It is capable of detection of a variety of low-density reactive gas phase species at a substrate position without the limitations, inherent to some of the optical techniques, such as the existence of suitable optical transitions of the radical or the molecule of interest. TIMS has been successfully applied for the radical density measurements, for example, in SiH₄–CH₄–H₂ glow discharge plasma,[2] Cl₂ plasma used for Si etching,[5] O₂ and N₂ plasmas,[1,6] and hot filament diamond chemical vapor deposition (CVD).[7] TIMS has been mainly utilized for measuring ground-state neutral species densities, however, it can also be used for identifying and measuring the density of excited species in a plasma. Recently, Agarwal *et al.* reported TIMS measurement of absolute densities of electronically excited N₂ in an inductively coupled N₂ plasma.[6] Although TIMS is a versatile technique, it requires a carefully designed differentially-pumped housing for the quadrupole mass spectrometer (QMS) and a proper calibration procedure to accurately determine the absolute number density of the radicals. Knowledge of the absolute density of various reactive species in a plasma is es-

sential for the validation of plasma chemistry models, since their results are often dependent on unknown reaction rates and reaction branching ratios.

There is an extensive scientific and industrial interest in hydrocarbon chemistry and carbon-based film-growth mechanisms. Hydrocarbon chemistry is widely studied because of its role in many industrial processes such as combustion and soot formation,[8,9] diamond and diamond like carbon film deposition,[10] or tritium redeposition in the divertor of the future fusion devices.[11] Moreover, hydrocarbon chemistry is also involved in the formation of (proto-) planets in the interstellar space[12] or it determines the composition of the hydrocarbon rich atmosphere of Saturn's moon Titan.[13] However, despite this interest, the hydrocarbon chemistry and carbon-based film growth mechanisms are still not well understood. The primary reason is the ability of carbon to form double and triple bonds leading to a large family of radicals and molecules produced in reactive environments. Due to the complexity of the hydrocarbon chemistry, the diverse species present in reactive hydrocarbon environments have to be identified experimentally.

We have implemented TIMS in a remote Ar/C₂H₂ expanding thermal plasma (ETP) chamber to detect the reactive hydrocarbon species and to understand their role in the plasma chemistry as well as in the growth mechanism of hydrogenated amorphous carbon (*a*-C:H) films. These films have advantageous properties such as high hardness, chemical inertness and optical transparency and are used as protec-

tive coatings on, e.g., magnetic storage disks, razor blades, or optical elements.[14] The remote Ar/C$_2$H$_2$ ETP is capable of fast (up to 70 nm/s) deposition of medium hard (hardness up to 14 GPa) *a*-C:H films without energetic ion bombardment of the film surface.[15] The application of energetic ion bombardment is, on the contrary, necessary in widely used radiofrequency plasma-enhanced CVD *a*-C:H deposition methods[14] in order to maintain good mechanical properties of the film. The ETP is primarily a radical source where the decomposition of the parent hydrocarbon molecule is ion induced. The contribution of electron-impact induced dissociation and ionization processes is negligible due to very low electron temperature (<0.3 eV).[16] The absence of ion bombardment of the film surface makes this process suitable for the study of the role of neutral radical species in the formation of *a*-C:H films.

The identification of the different reactive neutral species in the Ar/C$_2$H$_2$ ETP is of utmost importance. C, CH, and C$_2$ radicals have been previously measured using cavity ringdown absorption spectroscopy (CRDS).[17–19] However, the contribution of these radicals to the *a*-C:H growth (radical flux towards the surface multiplied by surface sticking probability) appears negligible under the conditions where hard *a*-C:H films are deposited. This has been attributed to high gas phase reactivity of C, CH, and C$_2$ with C$_2$H$_2$,[18] which results in a low density of these radicals close to the substrate. The role of the C$_2$H radical was also evaluated in previous study and its contribution to the growth was also small.[18] Therefore, other hydrocarbon radicals must be present in the Ar/C$_2$H$_2$ ETP, which lead to high-rate deposition of hard *a*-C:H films.

The first study of reactive neutral species in ETP by means of TIMS was performed in an Ar/H$_2$/SiH$_4$ ETP by Kessels *et al.*[20] This research followed previous mass spectrometry study of cationic silicon clusters in the same plasma.[21,22] The absolute densities of SiH$_3$ and SiH$_2$ radicals could be determined with a detection limit of ~1 ×10^{18} m^{-3}. The comparison to the CRDS measurements has shown good agreement between the TIMS and CRDS.[23] Atomic nitrogen was also measured by TIMS in an Ar/H$_2$/SiH$_4$/N$_2$ ETP,[24] again, in good agreement with two-photon absorption laser induced fluorescence measurements. The TIMS detection limit as well as the absolute accuracy of the density determination were limited at that time, since only single stage differential pumping was used, resulting in a high background signal in the mass spectrometer and necessitating a small sampling orifice to maintain low pressure.[20] In order to improve the TIMS detection limit, the mass spectrometry system used by Kessels *et al.* was upgraded by means of building a triply differentially pumped mass spectrometer housing, similar to the setups as proposed by Singh *et al.*[3] and Agarwal *et al.*[1]

The goal of this article is to present the design and implementation of the TIMS in the Ar/C$_2$H$_2$ ETP experimental setup and its ability to identify and measure more than 20 different hydrocarbon radicals and molecules formed in the Ar/C$_2$H$_2$ ETP. The article starts with a brief description of

the ETP deposition setup and a detailed description of the TIMS setup and the data collection procedure. Then two major issues related to the TIMS performance and absolute density calibration procedure are discussed. First, the background pressure variation in the TIMS setup induced by the mechanical beam chopper, including the model calculation (in the Appendix) and two possible correction methods, is treated. Second, the description of species density calibration, including the estimation of the near threshold behavior of electron impact ionization cross section and the effect of gas extraction in a transition regime between molecular and laminar flow, is given. In Sec. IV the concise Ar/C$_2$H$_2$ chemistry in the ETP is given followed by the description of the species identification and measurement procedure illustrated by the C and C$_3$H$_4$ species experimental data. The quality of the TIMS setup and the reliability of the calibration and measuring procedures are then demonstrated by a very good agreement between the C, CH, and C$_2$ relative measurements and CH absolute density measurement obtained by means of TIMS and CRDS. Finally, the experimental and literature data for all the measured hydrocarbon species are summarized in the Table I and examples of C$_3$, C$_3$H, and C$_3$H$_2$ species measurements are given.

II. EXPERIMENTAL SETUP

A. Expanding thermal plasma setup

The ETP has been described in detail elsewhere.[25] Briefly, an argon thermal plasma is remotely produced in a so-called cascaded arc, which expands into a low-pressure vessel as shown in Fig. 1. The argon ion and electron fluence emanating from the arc is fully controlled by the cascaded arc settings (Ar flow and arc current) and does not depend on the conditions in the reaction chamber. The argon flow through the arc is kept constant at 100 sccs (1 sccs=2.69 ×10^{19} particles/s). C$_2$H$_2$ is admixed in the gas expansion region by means of injection ring, located 5 cm from the arc nozzle. C$_2$H$_2$ is dissociated into different radicals through various ion-neutral charge transfer reactions and subsequent molecular ion-electron dissociative recombination reactions.[18] The *a*-C:H film is deposited on a temperature-controlled substrate (*c*-Si, glass, Al) situated 55 cm downstream from the injection ring. The vessel base pressure is maintained by a 1000 l/s turbomolecular pump and is below 10^{-6} mbar. During the plasma operation, Roots boosters (Edwards, EH2600, EH500A) are used with a pumping capacity of about 0.4 m^3/s. The pressure during plasma operation is kept constant at 0.29 mbar. The cascaded arc is situated in a movable housing such that the injection ring-substrate distance could be varied over the range of 25–55 cm.

B. Mass spectrometry setup

In this study, the original substrate holder is replaced by a three-stage molecular beam TIMS setup (with Hiden Analytical EPIC 300 probe, PSM upgrade with Bessel box energy analyzer) to measure the neutral species densities at the substrate plane (Fig. 1). Our design is similar to the one

TABLE I. Radicals and molecules identified by means of TIMS in an Ar/C_2H_2 ETP, their measured and reported IP, the electron energy used for they measurement and the EII cross section taken from the literature or estimated based on the arguments given in the text. The experimental error of IP is ±0.2 eV if not indicated otherwise. The literature source for IP values is Ref. 30 and references therein.

Species (amu)	Measured IP [eV]	Literature IP [eV]	$E_{electron}$ (eV)	$\sigma_I(E) \times 10^{-16}$ (cm^2)
C (12)	11.3	11.26	19	0.96/0.84[a]
CH (13)	10.5	10.64	19	0.72/0.90[a]
CH$_2$ (14)	10.5	10.35	14	0.31/0.43[a]
CH$_3$ (15)	9.9	9.84	13	0.26/0.37[a]
CH$_4$ (16)	12.6	12.61	17	0.60/0.51[a]
C$_2$ (24)	11.5	11.41	18	0.73[a]
C$_2$H (25)	11.7	11.61	15.5	0.45[a]
C$_2$H$_2$ (26)	11.4	11.40	14	0.31
C$_3$ (36)	12.1	11–13[b]	14	0.23[a]
C$_3$H (37)	9.7	9.8	15	0.59[a]
C$_3$H$_2$ (38)	9.2	8.7/9.15/10.43[c]	12	0.33[a]
C$_3$H$_4$ (40)	10.3	10.37	13	0.31[a]
C$_4$ (48)	11.9±0.5	12.6	18	0.61[a]
C$_4$H (49)	11.7±0.5	Not known	15	0.39[a]
C$_4$H$_2$ (50)	10.2	10.17	50	4.8[d]
C$_5$ (60)	11.4±0.5	12.3	17	0.63[a]
C$_5$H (61)	9.8	Not known	18	0.89[a]
C$_5$H$_4$ (64)	10.0	8.67/9.5/10.1[c]	13	0.35[a]
C$_5$H$_6$ (66)	10±1	8.0–9.3	13	0.35[a]
C$_6$H$_2$ (74)	Not measured	9.50	50	7.1[d]
C$_6$H$_6$ (78)	Not measured	8.1–9.9[c]	50	Not estimated

[a]Estimated value based on C_2H_2 EII cross section near threshold behavior.
[b]Spread of reported values.
[c]Values for different known isomers.
[d]Estimated on the basis of additivity rules.

described by Agarwal *et al.*[1] The details of the QMS housing are shown in Fig. 2. In this design we tried as much as possible to copy the shape and position of the original substrate holder in order to preserve the same experimental conditions as during previous deposition experiments so that direct comparison can be made with previous data. The species are sampled through a 0.8-mm-diam orifice at the position of the substrate plate. The sampling orifice is 45 mm off axis from the ETP source and experimental chamber axis. The neutral species densities may be slightly different at the center of the original substrate holder than at the off-axis orifice, but no correction is made to take into account the off-axis location of the sampling orifice. The sampling orifice is in line-of-sight with the QMS ionizer. The distance between the orifice and the center of the ionizer is 113 mm. This distance is minimized in our design to maximize the QMS signal intensity. The 1.6 mm inlet orifice for the second stage and the 4 mm inlet orifice for the third stage are at a distance of 40 and 75 mm, respectively, from the first orifice. The housing is designed such that, if required, all three apertures can be replaced and realigned on line of sight with the QMS ionizer. A mechanical shutter can be placed 10 mm in front of the substrate plane to block the ETP from reaching the substrate plane and to allow the investigation of species in the plasma background. No *a*-C:H films are deposited at the substrate plane when ETP is blocked with the shutter. Regular Ar/O_2 plasma cleaning steps are performed inbetween the Ar/C_2H_2 plasma experiments in order to prevent clogging of the sampling orifice with *a*-C:H deposits. Signal reduction due to the clogging was never observed. Three turbomolecular pumps with pumping capacities (for N_2) of 35, 300, and 56 l/s are used in the first, second, and third stage with estimated effective pumping speeds around 30, 120, and 10 l/s, respectively. The pressure is measured in the second and third stage by means of Penning ionization gauges. During plasma operation, the pressures in the second and third stages are below 5×10^{-7} and 1.2×10^{-7} mbar, respectively. The latter pressure in the third stage is rather high. As will be explained later, it is a consequence of high intensity of the sampled molecular beam. The second and the third stages can be hermetically separated from the rest of the setup by a mechanical shutter with a rubber O-ring (not shown in Fig. 2) located in the first stage. Therefore, the plasma chamber can be opened without exposing the entire QMS housing to the ambient atmosphere. A water-cooled 1-mm-thick copper plate is mounted at the plane of the first orifice to remove the heat induced by the plasma.

C. Data collection procedure

Several calibration steps are performed before the experiments. The space charge limited regime is checked as in Refs. 1 and 26. The QMS signal is proportional to the electron emission current up to 80 μA. An emission current be-
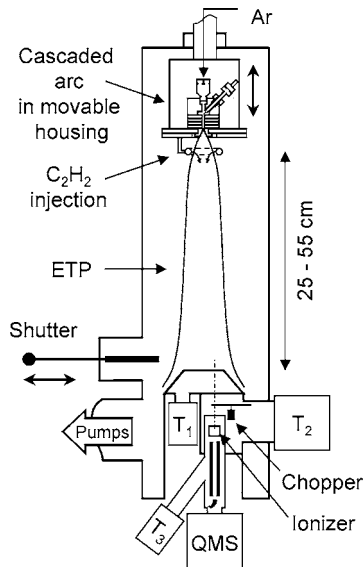
FIG. 1. Expanding thermal plasma experimental setup with the threshold ionization mass spectrometer (TIMS) at the position of the substrate holder.

FIG. 2. Detail of the threshold ionization mass spectrometer housing. The beam chopper is drawn only schematically.

low this value is always used. A drift of the electron energy setting with time is observed and hence the electron energy scale is calibrated with well-known ionization potentials (IPs) of argon, acetylene, and helium gases on a daily basis. To prevent any ions originating in the plasma from entering the QMS, its extractor lens potential is set at +30 V. Ultraviolet (UV) photons, also originating from the plasma, can result in the false counts measured by the detector of the QMS.[22] However, the Bessel box energy analyzer, used in our QMS, blocks effectively the line of sight between the sampling orifice and the detector.[20] Whenever the relative number densities of one or more species have to be compared the measurements are performed the same day in order to avoid errors due to a drift of, e.g., the detector sensitivity. The TIMS setup is regularly baked overnight in order to reduce the residual background pressure. The base pressure below 2×10^{-9} mbar is achieved in the third stage.

III. CALIBRATION PROCEDURE

A. Correction for beam chopper

As the neutrals sampled through the first orifice pass through the second orifice a molecular beam is formed in the TIMS. The molecules in the beam pass through the third orifice and enter the QMS ionizer where they are detected. The beam species have not collided with any part of the TIMS housing on their way to the ionizer. The molecules, which are not in the beam, undergo several collisions with the TIMS housing and are either pumped away in the first or second stage or enter the third stage where they contribute to the background pressure. These neutrals will be responsible for the background component of the QMS signal. A mechanical chopper (shown only schematically in Figs. 1 and 2) located in the second stage is used to block the beam and allows the measurement of the background component of the QMS signal. The chopper has six blades, the outer diameter
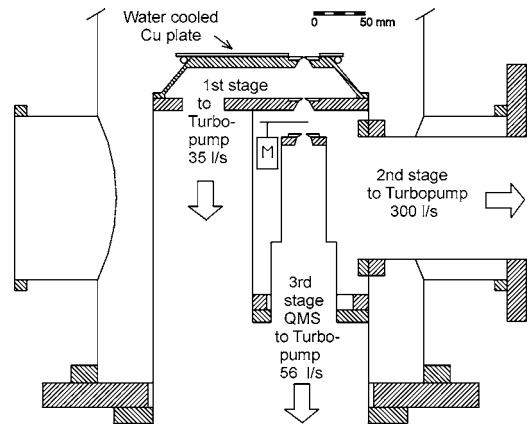
of 70 mm and the chopper blade blocks the beam 9 mm above the third orifice. The chopper is mounted on the axis of a computer controlled stepper motor (Caburn, SM32-UHV).

However, a significant change of the pressure in the third stage is observed between the chopper blocking and chopper open positions (e.g., a seven times increase in the case of argon gas at the vessel pressure of 29 Pa). The pressure increase is caused by the beam species, which after passing the ionizer collide with the QMS parts and contribute finally to the background pressure in the third stage. Since the distance between the first and third orifice is small, the flux of beam species into the third stage is relatively large. This, combined with a very low effective pumping speed in the third stage, results into a high additional background pressure in the third stage originating from beam species. In the Appendix we present a model calculation, based on the molecular flow conditions, dealing with this additional background and illustrating its significance. With a chopper modulating the pressure in the third stage, the net beam component of the QMS signal cannot be obtained by subtracting the signal measured with the chopper in the blocking position from signal measured with chopper in open position (except for radicals with high surface reaction probability, due to which they are effectively removed from the background in the third stage and have therefore negligible background). The background pressure modulation could be avoided, if the chopper would be situated in the third instead of the second stage. The location of the chopper in the third stage is in our case impossible due to geometrical limitations.

The optimal method of eliminating the background pressure variation in the third stage is the use of continuous chopping. Due to the small effective pumping speed in the third stage, the residence time of the background species in this stage is relatively long ($\tau \sim V_3/S_3$, where V_3 is the volume and S_3 the effective pumping speed of the last stage). When the beam is chopped with a chopping period significantly shorter than the residence time, the background pressure is not able to track the beam modulation and the ac component of the QMS signal is solely due to the beam
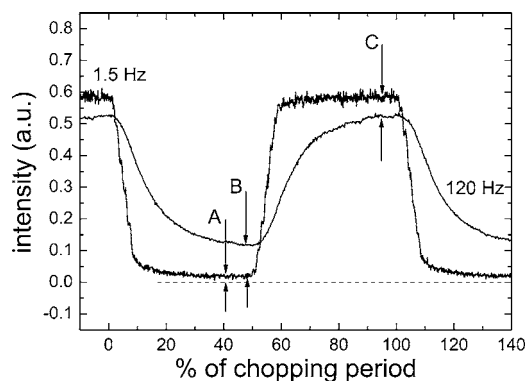
FIG. 3. Comparison of the QMS signals at 1.5 and 120 Hz chopping frequency measured with argon gas in the vacuum chamber. The *x* axis scale is in % of the chopping cycle. The increase of the background signal at high chopping frequency is clearly visible when A and B are compared. The difference between B and C indicates that chopper influences the conductivity in the second stage. The time delay of 0.8 ms observed on the signal is the artifact of the analog output of the HIDEN instrument.
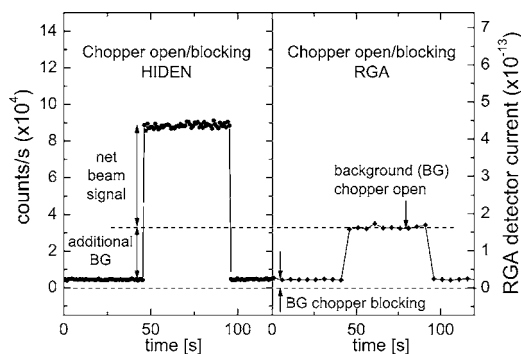

FIG. 4. Chopper open/chopper blocking measurement of acetylene gas performed with HIDEN mass spectrometer and RGA. The RGA is able to measure partial pressures in the third stage of the TIMS housing. The chopper open/blocking ratio of RGA signal is used to scale the HIDEN measured background signal intensity.

species. The measurement with fast chopping performed after the QMS upgrade (Fig. 3) demonstrates the influence of the chopping speed on the QMS signal for argon gas. The background component rises at higher chopping frequency (see the difference between A and B in Fig. 3) with a slightly asymmetric behavior (see the difference between B and C), most probably due to the conductivity limits induced by the chopper blades. The fast analog output available at the HIDEN instrument was used to obtain these data. The time delay of 0.8 ms observed on the signal is an artifact of this analog output. Note that using the fast chopping procedure, the net beam signal is also corrected for possible products of thermal dissociation of the parent molecules on the filament in the QMS ionizer.

An alternative method of obtaining the proper background component of the QMS signal is used throughout this article. The increase of the background partial pressure of the species of interest in the third stage is measured by means of an additional residual gas analyzer (RGA) mass spectrometer (RGA, Kurt J. Lesker, AccuQuad 200D). The partial pressure measurement is performed in the chopper open and blocking positions and the RGA signal ratio between these two measurements is used to scale the background signal measured with the QMS, (see Fig. 4). In this way the proper background of the stable species, such as C_2H_2 or C_4H_2, when the chopper is open, can be obtained.

Some limitations have to be taken into account with this approach. It is not possible to measure the background pressure of reactive radicals and also species with a third stage background density under the detection limit of the RGA. The latter limitation can be overcome since we have found experimentally that background variation for stable species is, at a fixed vessel pressure, only dependent on the species molecular weight and can hence be calibrated by known gases and extrapolated for the other species. The former limitation is negligible in the case where the measured radical has a high surface reaction probability (e.g., the case of C, CH, C_2, or C_2H radicals). Then the background pressure in

the ionizer is negligible and the measured signal can be fully attributed to the beam species. In this case it is not necessary to use the beam chopper and hence these radicals are measured with chopper only in the open position. For radicals with a lower surface reaction probability (e.g., the CH_2 and CH_3 radicals) the background species will probably contribute to the measured signal. However, we measured these radicals without correction for the background signal as well. The background signal for all measured stable species was never higher than 50% of the total measured signal (cf. Fig. 4 for C_2H_2). Therefore, the resulting signal (and finally also density) of radicals with a lower surface reaction probability can be overestimated by no more than a factor of 2, which is an acceptable error considering all other experimental uncertainties.

B. Calculation of absolute density of neutrals

In the calibration procedure one wants to relate the measured signal with an absolute number density of measured species in the reactor. The detector signal $S_i(E)$ for species i at electron energy E is related to the density of species i in the QMS ionizer by:

$$S_i(E) = \beta \cdot T(m_i) \cdot \theta(m_i) \cdot l_{\text{ionizer}} \cdot I_e \cdot \sigma_i(E) \cdot n_{i,\text{beam}}^{\text{ionizer}}, \qquad (1)$$

where β is the extraction efficiency of the ions from the ionizer, $T(m_i)$ is the species mass-to-charge ratio dependent transmission efficiency of the energy filter (Bessel box) and quadrupole mass filter, $\theta(m_i)$ is the species mass-to-charge ratio dependent sensitivity of the detector, l_{ionizer} is the length of the ionizer cage, I_e is the emission current in the ionizer, $\sigma_i(E)$ is the energy dependent electron impact ionization (EII) cross section of the relevant ionization process, and $n_{i,\text{beam}}^{\text{ionizer}}$ is the beam density of species i in the ionizer. The unknown density of a given species i in the ionizer can be determined, when the species j of known density is measured under the same conditions and with the same QMS settings. Taking the ratio of two Eqs. (1) for both species:[4]

$$n_{i,\text{beam}}^{\text{ionizer}} = \frac{S_i(E) \cdot T(m_j) \cdot \theta(m_j) \cdot \sigma_j(E)}{S_j(E) \cdot T(m_i) \cdot \theta(m_i) \cdot \sigma_i(E)} n_{j,\text{beam}}^{\text{ionizer}}. \qquad (2)$$

The product $T(m) \cdot \theta(m)$ for a given species depends on the geometry and the ion optic settings of the QMS and it can be calibrated by measuring mixtures of gases with known densities. The $T(m) \cdot \theta(m)$ product drops out, when species i and j have the same mass. When the gas extraction is effusive, the gas composition is preserved and the beam density in the ionizer is proportional to the vessel density for every species regardless of their mass or collision cross section [cf. Eq. (A3) in the Appendix]. Under these conditions, the density at the sampling orifice can replace the ionizer density in Eq. (2) and the absolute density of species i at the sampling orifice is obtained.

C. Electron impact ionization cross section

The absolute values of the EII cross sections or at least the ratio of EII cross sections has to be known in the calibration procedure. They have been measured for most of the stable gases used or detected in this study, and the most recent and revised data are listed in Refs. 27 and 28. The EII cross sections have also been measured for the CD_y ($y = 1-3$) radicals[29] and the C atom.[30] For other hydrocarbon radicals the EII cross sections are not known and assumptions concerning their values have to be made. It has been shown that above electron energy of 20–30 eV additivity rules can be applied and the total EII cross section of hydrocarbon molecules C_xH_y (with x up to 5 and y up to 12) scales linearly with the amount of C atoms.[31] Moreover it has been shown that the EII cross section scales in a similar way with the number of H atoms in the radical/molecule, when the number of C atoms is fixed.[31] These additivity rules are used here to estimate the EII cross sections of C_4H_2 or C_6H_2 molecules at the electron energy of 50 eV. It is assumed that the ratios of partial to total EII cross sections $\sigma_{C_4H_2^+}^{C_4H_2}/\sigma_{C_4H_2}^{\text{total}}$ and $\sigma_{C_6H_2^+}^{C_6H_2}/\sigma_{C_6H_2}^{\text{total}}$ are equal to the $\sigma_{C_2H_2^+}^{C_2H_2}/\sigma_{C_2H_2}^{\text{total}}$ ratio at 50 eV. Unfortunately the radical species has to be detected with electron energies close to the ionization threshold, where additivity rules cannot be applied and some "threshold law" has to be assumed. In order to be able to estimate the near threshold EII cross sections, the experimental data available for CD_y ($y = 1-4$), CH_4, C_2H_2, C_2H_4, C_2H_6, and C_3H_8 species are compared. The electron energy scales were shifted in the way that IPs of these species overlap. All of them, except for the C_3H_8 molecule, have similar threshold behavior without any trend indicating the additivity rules being operative. Moreover the CD_y ($y = 1-4$) data, measured on the same experimental setup, shows almost perfect overlap. Therefore, we approximate the unknown EII cross sections of the measured radical at the electron energy ΔE above the radical IP by the C_2H_2 EII cross section at the same ΔE above the IP of C_2H_2. Since only the ratio of EII cross sections is used in Eq. (2), the error due to this approximation will be the systematic error depending only on how much the near threshold EII cross section behavior of the radical differs from the one of the C_2H_2 molecule. The electron energy values used for tracking the species behavior under different conditions and estimated EII cross sections are listed in Table I. The estimate is done also for radicals for which the EII cross section is available (C, CH, CH_2, CH_3 and CH_4) and the agreement with reported values is within 50%. We expect that the uncertainty due to estimated EII cross section for the other radicals is also within 50%.

D. Gas extraction

The extraction of the gas at static pressure in the reactor chamber through the orifice into the low-pressure region has two limiting cases characterized by the Knudsen number $Kn = \lambda/d$, where λ is the mean free path of the neutrals in the reactor chamber and d is orifice diameter.[32] In the case the pressure is low and $Kn > 1$, the extraction is effusive and can be treated by kinetic theory of the gases. The species densities on the orifice axis (beam centerline) are then proportional to the species densities in the reactor chamber and can be calculated by Eq. (A3) given in the Appendix. On the other hand, if $Kn < 0.01$, the flow through the orifice is in the continuum limit, forming a free jet with supersonic velocities of the gas, and gasdynamics can be applied to predict, e.g., the density and velocity distribution in the extracted gas.[33] However, different composition distortion effects such as pressure diffusion or Mach number focusing have to be taken into account in this case.[34] When effusive and continuum extractions are compared, assuming the same gas flow through the orifice, the continuum extraction provides (up to two times) higher beam intensities on the beam centerline.[33] The beam intensity on the centerline can be reduced by the collisions of the species in the beam with the background species, e.g., in the first stage of the mass spectrometer. The beam species scattering and reduction of beam intensity at elevated pressures due to the collisions was observed, e.g., by Agarwal *et al.*[1]

The diameter of the first sampling orifice of 0.8 mm is at the chamber pressure of 29 Pa bigger than the mean free path of 0.23 mm (for Ar at 298 K gas temperature), giving the Knudsen number of $Kn = 0.28$. The relatively large 0.8 mm orifice is selected to have high beam intensity and hence increased sensitivity to detect low-density radicals such as CH_2 (with a count rate of only 10 counts/s). Still, reasonably low background pressure in the third stage is maintained. Since the extraction is in the transition regime between free molecular limit and continuum limit, the possible effects of composition distortion has to be checked. In general these effects are collision related and hence they will be dependent on the mass difference between the species of interest (minority species) and argon (majority species) and on the difference between the species of interest-argon collision cross section compared to argon–argon collision cross section. In Fig. 5 we show the QMS signal as measured for H_2 (collision diameter 2.76 Å, as listed in Ref. 35), He (2.66 Å), CH_4 (3.81 Å), C_2H_2 (4.4 Å, estimated), O_2 (3.49 Å), and Kr (3.59 Å) divided by the ionization cross section and the species number density calculated from the gas flow (typically
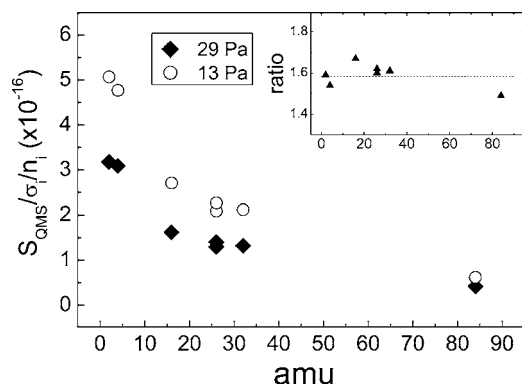
FIG. 5. QMS signals of H_2, He, CH_4, C_2H_2, O_2, and Kr, divided by their electron impact ionization cross section and their vessel density, at two different pressures of 29 and 13 Pa. Argon is used as a dilution gas. Insert shows the ratio of the signals.

7 sccs) and pumping speed of 0.4 m³/s. Two measurements are done at a total pressure of 29 Pa (Kn=0.28) and 13 Pa (Kn=0.63) for every gas. The pressure difference is achieved by variation of the flow of argon (100 and 25 sccs), which is used as a dilution gas. The measurement at 13 Pa gives higher signals, which is due to the relatively higher partial pressures of the gases in the reaction chamber, since the pumping speed of the Roots blower is reduced at lower pressures in this pressure region. The data points are on a smooth curve, which indicates that the difference of collision cross section has only a small effect on the beam composition. The value decreases with increasing molecular weight, which is dominantly the effect of mass dependent transmission function of the QMS, $T(m_i) \cdot \theta(m_i)$ product in Eq. (1), and possibly also due to mass dependent composition distortion effect. The ratio between the measured values for the two pressures (two Knudsen numbers) is almost constant (within the accuracy of the flow controllers and the QMS and RGA signals), indicating that the beam composition distortion is still very small, even under Kn=0.28 conditions.

From this discussion it follows that the calibration as described in the Sec. III B can also be used for the measurements performed with the 0.8 mm diameter of the first orifice and chamber pressure of 29 Pa. The C_2H_2 signal (corrected for the background as shown in Fig. 4) at an electron energy of 14 eV, measured at C_2H_2 partial pressure of 2 Pa and total pressure of 29 Pa, is used to calibrate the number densities of different hydrocarbon radicals, using Eq. (2). The values of correction factor $T(m_j) \cdot \theta(m_j)/T(m_i) \cdot \theta(m_i)$ used in Eq. (2) can be determined from the measured trend in Fig. 5.

Note Added in Proof: An additional issue has to be considered if the diameter of the sampling orifice is comparable or bigger than the particle mean free path and radicals with high surface reactivity are measured. These radicals have a density gradient close to the surface, which depends on their sticking probability, and due to this gradient and due to the partial convective flux into the sampling orifice, the density measured will equal the radical density slightly above the substrate plane. For this reason we recommend to use, when-

ever the signal intensity allows, an orifice with diameter smaller than particle mean free path.
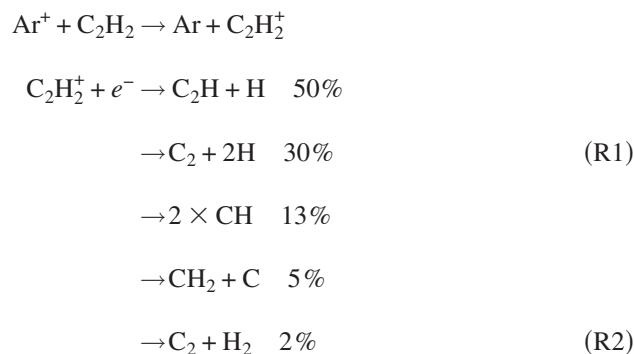
E. Systematic errors

The largest source of error in the calibration procedure are the unknown EII cross sections with the above estimated accuracy of <50%. The additional sources of errors such as the composition distortion in the extraction or possible effect of gas temperature on the measured signal are estimated to be smaller than 25%. We use these possible systematic errors to estimate an upper ($n \times 1.5 \times 1.25$) and lower limit ($n \times 0.5 \times 0.75$) of the density n obtained in the calibrating procedure. Moreover it is expected that for similar species with similar mass and structure (e.g., C_3, C_3H, and C_3H_2) the systematic error due to the unknown EII cross sections are similar. As a consequence, the density ratio for similar species is probably more reliable than the determined absolute density values.

IV. RESULTS AND DISCUSSION

A. Concise Ar/C_2H_2 ETP chemistry

The main goal of this article is to present the TIMS setup and to show its capability to detect a variety of hydrocarbon radicals. Still it is worth to mention the basic plasma chemistry, which leads to the production of these radicals. The primary dissociation of acetylene is induced by charge transfer (CT) reaction with an argon ion followed by dissociative recombination (DR) of the $C_2H_2^+$ ion with an electron:[36,37]

$$Ar^+ + C_2H_2 \rightarrow Ar + C_2H_2^+$$

$$C_2H_2^+ + e^- \rightarrow C_2H + H \quad 50\%$$

$$\rightarrow C_2 + 2H \quad 30\% \tag{R1}$$

$$\rightarrow 2 \times CH \quad 13\%$$

$$\rightarrow CH_2 + C \quad 5\%$$

$$\rightarrow C_2 + H_2 \quad 2\% \tag{R2}$$

with the DR branching ratios experimentally measured by Derkatch *et al.*[38] for the ground state $C_2H_2^+$ ion. It should be noted that $C_2H_2^+$ ion and the radical products of reaction (R2) are formed (highly) rovibrationally excited as a result of the difference between ionization potentials of argon (15.76 eV) and C_2H_2 (11.4 eV). The products of reaction (R2) can be further dissociated in another CT and DR step or can react with the unconsumed C_2H_2 or other hydrocarbon molecules or radicals. The electron impact induced dissociation can be neglected because electrons are cooled to well below 0.3 eV[16,39] in the expansion. In previous work it was shown that the plasma composition depends on the ratio between the C_2H_2 flow and argon ion and electron fluence emanating from the cascaded arc.[18] If this ratio is lower than one, the acetylene is decomposed into C, CH, C_2, and C_2H radicals. For ratios much higher than one the radical-neutral reaction
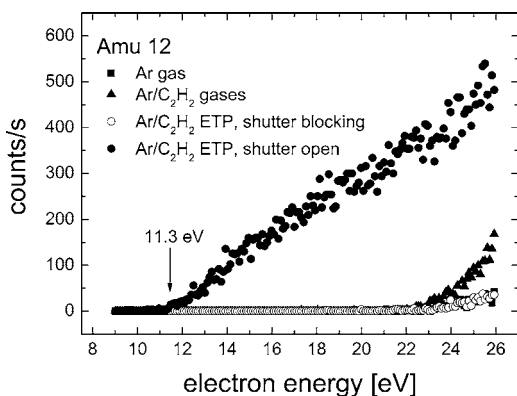
FIG. 6. QMS signal at m/e ratio of 12 as function of electron energy. Vessel pressure 29 Pa, arc current 48 A, ring-substrate distance 25 cm, and C_2H_2 flow 7 sccs.

FIG. 7. QMS signal at m/e ratio of 40 as function of electron energy. Vessel pressure 29 Pa, arc current 48 A, ring-substrate distance 55 cm, C_2H_2 flow 18 sccs.

will follow the primary CT and DR steps. Under these conditions C_4H_2, C_6H_2, and C_6H_6 molecules were measured in the plasma background by means of a residual gas analyzer.[18] In the rest of this article we present measurements concerning more than 20 hydrocarbon radicals and molecules as detected using the TIMS setup. Among detected species are all carbon containing products of reaction (R2): C, CH, CH_2, C_2, and C_2H radicals, and also the possible products of reaction of these radicals with C_2H_2: C_3, C_3H, C_3H_2, C_4, and C_4H radicals.

B. Species identification

The TIMS technique utilizes the difference of the electron impact ionization threshold of the given radical and the electron impact dissociative ionization (DI) threshold of the parent molecule, which is typically several electron volts bigger. Therefore, the proper selection of the electron energy in the QMS ionizer allows direct radical measurement. When the measurements are performed with varying electron energies at fixed mass, both the IP of the radical as well as the appearance potential of the ion from the possible DI of the parent molecule can be determined and used for the species identification. We identify the species by means of four electron energy scans performed at a fixed mass of interest. In the first scan only the argon gas is used in order to detect any possible background pollution in the vessel or in the QMS itself. The second scan is performed with argon and acetylene gases. The appearance of C, CH, CH_2, C_2, and C_2H radicals due to DI of C_2H_2 and also the presence of these radicals due to possible thermal dissociation of C_2H_2 on the filament in the ionizer can be checked. The third measurement is done with Ar/C_2H_2 plasma and with the shutter placed in front of the sampling orifice to block the plasma from reaching the substrate plane (cf. Fig. 1). The final scan is measured with the plasma running and without the shutter blocking the plasma. The shutter is used in order to distinguish between reactive radicals, present only in the plasma, and stable or less reactive plasma chemistry products, which can also be found in the plasma background and hence also under the shutter. It might reveal a possible role of measured
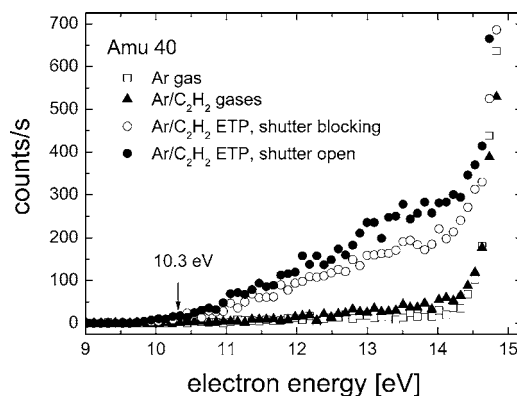
species in the deposition process because no deposition of a-C:H film was observed under the shutter. The chopper in the second stage of the QMS setup is kept open for all the scans to avoid modulation of the background pressure in the third stage. With the chopper open and the shutter in front of the sampling orifice the background pressure of the stable species in the third stage is almost unchanged and possible thermal dissociation products can be observed and their contribution to the signal measured without the shutter correctly subtracted. Only in the case of the C_2H radical measurement the weak signal due to C_2H formed in the thermal dissociation of C_2H_2 was observed at highest C_2H_2 flows used and was corrected for. The electron energy scans are in most of the cases performed with the arc lowered to an injection ring-substrate plane distance of 25 cm, since the radical density, and therefore the count rate, is higher.

Two examples are given in Fig. 6 (the C radical, 12 amu) and Fig. 7 (stable C_3H_4 molecule, 40 amu). Argon gas measurement at 12 amu gives zero signal except for the small background appearing at electron energies above 22 eV. When Ar and C_2H_2 gases are present, the signal at electron energies above 22 eV increases as a result of carbon ion formation in the DI of acetylene. When the plasma is turned on but the shutter is blocking it, the signal due to DI of C_2H_2 disappears. This is the result of almost complete C_2H_2 consumption in the plasma. When the shutter is removed carbon atoms, now originating from the plasma, are responsible for the signal with IP at 11.3±0.2 eV, in good agreement with the reported value of 11.26 eV.[40] In Fig. 7 scans at mass 40 are shown. When the plasma is not running a weak background of unknown origin is observed. Next to it, argon contributes to the signal at electron energies above 14.5 eV. The IP of argon is 15.76 eV, but since the electron energy distribution function has a full width at half maximum (FWHM) of about 0.5 eV and the argon density is several orders of magnitude higher than the radical densities, it leads to high count rates already starting 1 eV below its IP. When the plasma is running the signal due to the species with IP at 10.3±0.2 eV is observed, even with shutter blocking the first orifice. Propyne, the linear C_3H_4 molecule ($CH_3-C\equiv CH$),
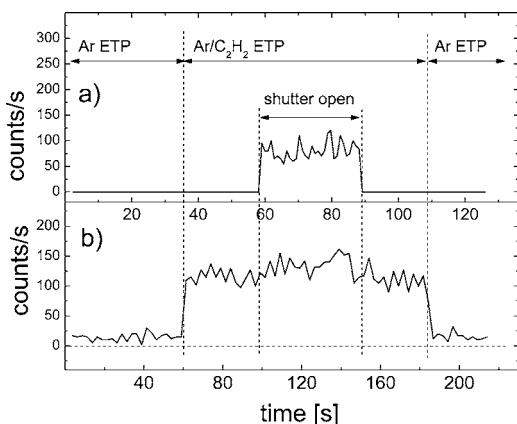
FIG. 8. QMS signal at the fixed mass collected at three different conditions. First the argon ETP plasma is running with the shutter in front of the substrate plane blocking the plasma. Then the acetylene gas is injected into the ETP and finally the shutter is removed. A measurement of C at 19 eV electron energy (a) and C_3H_4 molecule at 13 eV electron energy (b) are shown here. The chopper is in the open position.
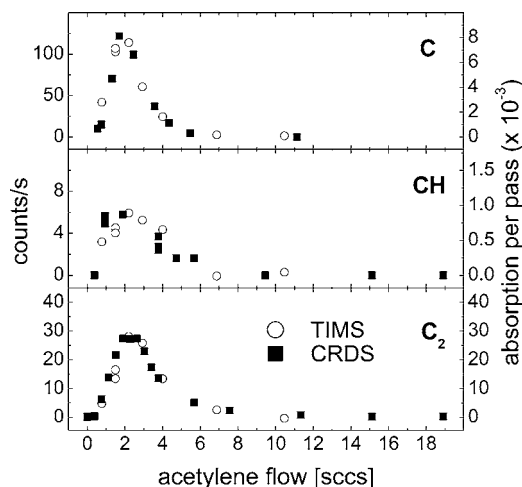

FIG. 9. C, CH, and C_2 radical measurements as function of acetylene gas flow into the reactor. The arc current of 48 A and argon gas flow of 100 sccs is used. The TIMS results are compared with CRDS absorption measurement of these radicals performed in the past under the same conditions.

is responsible for this signal, since its reported IP is 10.36 eV,[40] and as a stable molecule it is also present in the plasma background.

When measuring the species under different conditions, only one electron energy is selected and the QMS signal is measured for an Ar ETP and Ar/C_2H_2 ETP with the shutter and Ar/C_2H_2 ETP without the shutter blocking the first orifice (cf. Fig. 8). The measurement with Ar ETP is used as a baseline and the measurement with shutter blocking the Ar/C_2H_2 ETP shows the presence of the hydrocarbon species in the plasma background. The measurement done without shutter and corrected for the baseline is used to represent the species relative densities. The two sigma statistical error is calculated from the measured data (usually more than ten points are collected for every condition). The integration time is between 0.2 and 1 s per point, depending on the radical count rate. The C, CH, and C_2 radicals were measured in this way as a function of the C_2H_2 flow at the arc current of 48 A using an electron energy of 19 eV for the C and CH radicals and 18 eV for the C_2 radical. The results are shown in Fig. 9 together with the CRDS measurement of C, CH, and C_2 performed with the laser beam passing 30 mm above the substrate plane.[17–19] The relative agreement between TIMS and CRDS measurements is excellent and corroborates that the TIMS measurements under different plasma conditions are comparable.

Next to the relative intensities also absolute number densities at measured maxima ($\sim$2 sccs C_2H_2 flow, cf. Fig. 9) can be determined based on the TIMS measurements and are $2.8^{+2.5}_{-1.8} \times 10^{17}$, $1.9^{+1.7}_{-1.2} \times 10^{16}$, and $1.1^{+1.0}_{-0.7} \times 10^{17}$ m^{-3} for C, CH, and C_2 radicals, respectively. The CH density determined based on the CRDS measurements under the same experimental conditions, but 3 cm above the substrate plane, was 6.8×10^{16} m^{-3}. The TIMS determined CH density agrees with the CRDS result very well if we consider the fact that the density of the reactive species with nonzero surface reaction probability drops at the vicinity of the surface.[41,42]

Since the TIMS measures the species densities at the substrate plane, it provides lower values than CRDS measurement in the gas phase. The C density cannot be compared since only the metastable $1s^2\,2s^2\,2p^2\,^1S_0$ state 2.52 eV above the ground state was measured by CRDS[19] with the metastable carbon density around 5×10^{15} m^{-3}. However, the relative agreement between carbon measurements shown in Fig. 9 fully corroborates our conclusion discussed in previous work[19] that the metastable carbon measurements, under Ar/C_2H_2 ETP conditions, are also representative of the C ground state.[19] The C_2 maximum density determined by CRDS is 3.5×10^{18} m^{-3}. (The C_2 density calculation from the CRDS data was checked several times. In our previous article[19] we mentioned erroneously the maximum C_2 density as being more than ten times smaller). Such a high C_2 density seems too be overestimated because it would result, with C_2 sticking probability close to unity,[43] in much faster growth rate than measured. Therefore, the comparison between the TIMS and CRDS determined densities of C_2 are not done. Further analysis is required to understand why the CRDS measurement provides such a high C_2 density.

Table I summarizes all the detected radicals and stable species and compares the measured IP with literature values taken from the *NIST Chemistry Webbook*.[40] The measured IP is obtained from a linear fit to the ion signal in the near threshold region of the electron energy scan. Only in the case of the CH_4 molecule (IP of 12.61 eV) is the fact that the slope of the ion signal changes at around 13 eV taken into account.[44] For all the measured IP of stable species the agreement with the reported literature values is within 0.2 eV and we expect that the radical IPs are measured and determined with the same accuracy. Indeed, the measured IP values obtained for CH_y ($y=0-3$), C_2, and C_2H radicals are within this error. In the case of C_4, C_4H, C_5, and C_5H_6 species a shorter integration time was used leading to a larger error in IP determination. The electron energy used for species measurement under different conditions and EII cross
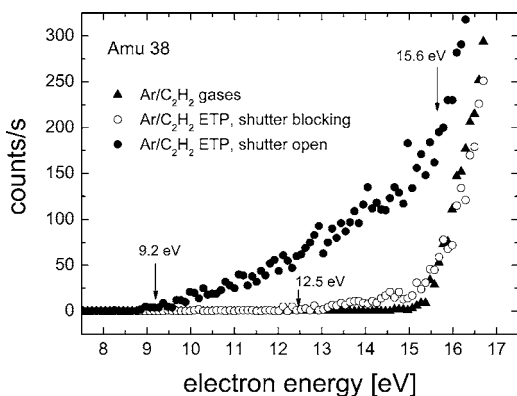
FIG. 10. QMS signal at *m*/*e* ratio of 38 as function of electron energy. Vessel pressure 29 Pa, arc current 48 A, ring-substrate distance 25 cm, and C_2H_2 flow 18 sccs.

FIG. 12. QMS signal at *m*/*e* ratio of 37 as function of electron energy. Vessel pressure 29 Pa, arc current 48 A, ring-substrate distance 25 cm, and C_2H_2 flow 18 sccs. Electron energy scale enlarged to show 12.3 eV change of slope.

sections used for the density calibration are also listed in Table I.

Most of the hydrocarbon species with more than two carbon atoms have more isomers and the experimentally obtained IP can help to identify which of the isomers is present in the Ar/C_2H_2 ETP. Figure 10 presents the electron energy scans at 38 amu (the C_3H_2 radical). Eight possible C_3H_2 isomers are known[45] and the IP was measured or calculated for the three most stable ones: propargylene (8.7–8.8 eV), cyclopropenylidene (9.15±0.03 eV), and propadienylidene (10.43±0.02 eV).[46] The measured IP of 9.2±0.2 eV suggests that the cyclopropenylidene radical, the most stable C_3H_2 isomer, is formed and detected. The same C_3H_2 isomer has been measured by means of TIMS in low-pressure $C_2H_2/O_2/H_2$ flames by Boullart *et al.*[47] The C_3H_2 appearance potential (AP) at 12.5 eV measured when the shutter is placed in front of the substrate can probably be attributed to the dissociative ionization of the penta-1,4-diyne (C_5H_4) molecule.[40] The C_5H_4 was also detected in Ar/C_2H_2 ETP under these conditions and a reported AP of $C_3H_2^+$ from C_5H_4 is 12.3 eV. The Ar^{38} isotope is responsible for the signal above an electron energy of 15.6 eV.

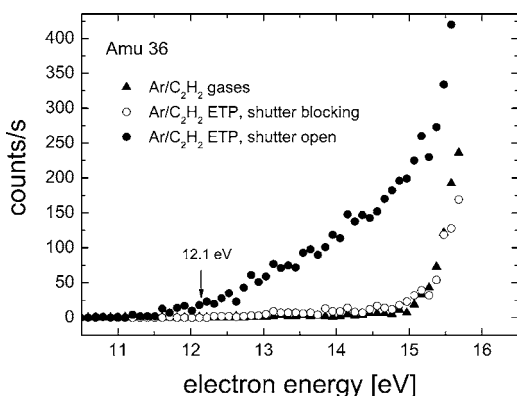Figure 11 shows the electron energy scans at 36 amu (the

FIG. 11. QMS signal at *m*/*e* ratio of 36 as function of electron energy. Vessel pressure 29 Pa, arc current 48 A, ring-substrate distance 25 cm, and C_2H_2 flow 18 sccs.
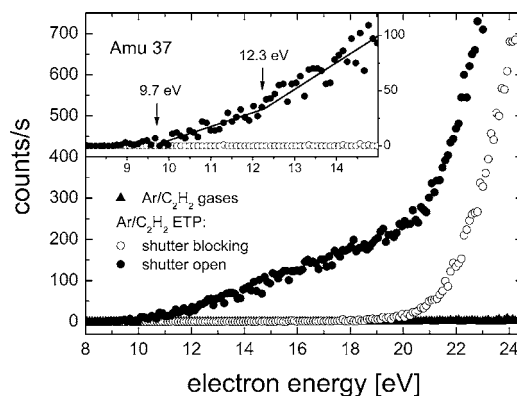
C_3 radical). The C_3 radical is one of the dominant products of the laser ablation of graphite[48] and was also detected in interstellar environments.[49] Moreover, it was predicted to be abundant in the Ar/C_2H_2 ETP by Mankelevich *et al.*[50] Two isomers, cyclic and linear C_3, can be formed.[49] The theoretical (for linear C_3) and experimental (without distinction) IP determinations show a large spread of the values in the range between 11 and 13 eV (cf. an overview in Ref. 51). The value measured here, 12.1±0.2 eV, is the same as measured by Wyatt and Stafford.[52] Unfortunately, it cannot be resolved at this moment which isomer is observed.

Two isomers, linear and cyclic, are also known for the C_3H radical.[53] The IP of the C_3H radical was measured by Boullart *et al.*[47] providing the value of 9.8 eV. However, the isomerization of C_3H was not identified. The C_3H radical measurement under Ar/C_2H_2 ETP conditions is shown in Fig. 12 with an IP of 9.7±0.2 eV, in good agreement with the result of Boullart *et al.* Both our electron energy scan and the one measured by Boullart *et al.* show the change of the slope at an electron energy around 12 eV. In the measurement performed with the shutter blocking the first orifice the signal starts to appear at electron energies above 19 eV with a strong increase above an electron energy of 22 eV. Regarding the intensity of the signal above 22 eV only the C_4H_2 or C_6H_2, the most abundant plasma chemistry products, can be possible candidates for the parent molecule. We used a homemade liquid nitrogen cold trap in order to collect C_4H_2 gas from the background of the ETP. The APs of C_3H^+, C_4^+ and C_4H^+ from dissociative ionization of C_4H_2 were 22.7, 23.2, and 17.3 eV, respectively, indicating that the C_4H_2 molecule could be the parent species. However the contribution from the DI of the C_6H_2 cannot be excluded. The C_5H_4 molecule could be the candidate for the parent molecule with a C_3H^+ appearance potential around 19 eV.

The identification of the other species listed in Table I was straightforward and was performed in the same way as the above-mentioned radicals. Still some interesting features were observed. The C_5H_4 molecule with its IP of 10±0.2 eV is probably penta-1,4-diyne with a reported IP of 10.1 eV.[40]

The signal at mass 63 amu ($C_5H_3^+$) was only due to dissociative ionization of the C_5H_4 molecule with measured AP of 12.5 ± 0.3 eV. The C_5H_4 molecule has a peculiar behavior in the sense that its density (signal at a fixed electron energy and 64 amu) is stable when measured with the plasma running and without the shutter blocking the plasma from reaching the first orifice. However, at the moment the shutter is used to block the plasma, the C_5H_4 signal, which is still present, starts to increase with time. A possible explanation can be the temperature dependent production of C_5H_4 on the hot surface of the shutter, which is heated by the ETP.

After a successful identification of the radical and stable species in the Ar/C_2H_2 ETP their densities should be studied under different experimental conditions in order to gain more knowledge about the plasma chemistry and about possible *a*-C:H film growth precursors. The results of such study are beyond the scope of this article and will be published elsewhere.[54,55]

V. CONCLUSIONS

A newly designed and built triple stage TIMS has been integrated in the Ar/C_2H_2 ETP setup at the position of the substrate holder. The sampling orifice is situated at the substrate plane allowing the direct density measurement of the radical species arriving at the surface. The mechanical chopper placed in the second stage is used to separate the beam and background components of the ion signal. Additional corrections have to be made to compensate for the strong background pressure oscillations in the third stage connected with the chopper position. Density calibration procedure including compensation for the background oscillation is proposed and the influence of collisions in the extracted beam are discussed. The apparatus performance and density calibration procedure are validated by comparing relative (C, CH, and C_2) and absolute (CH) densities measured by TIMS and CRDS. Moreover, a total of 21 hydrocarbon molecules and radicals are successfully identified and the IP are measured for most of them. As an example the electron energy scans at 36 amu (C_3), 37 amu (C_3H), and 38 amu (C_3H_2) are shown.

APPENDIX: MODEL CALCULATION

In the article of Singh *et al.*[3] the beam-to-background ratio calculation was performed for the situation when the additional background due to the beam species can be neglected. Their calculation is extended here for the situation,

in which the molecular beam is a significant source of the background pressure in the last stage of the TIMS setup. The calculation is done for a system with three stages. As in the paper of Singh *et al.*, free molecular flow conditions are assumed in all stages. Then the residual background density in the *m*th stage can be calculated as:

$$n_m^{\text{background}} = n_0 \prod_{i=1}^{m} \frac{C_i}{S_i}, \qquad (A1)$$

where n_0 is the number density of the species of interest, C_i is the conductivity of the aperture between the $(i-1)$th and the ith stage, and S_i is the effective pumping speed of the species due to the vacuum pump in the ith stage. This residual background can be greatly reduced by increasing effective pumping speeds or reducing conductivities between the individual stages (reducing aperture sizes). In the case all apertures are aligned, as in the case of the line-of-sight TIMS setup, a molecular beam is formed. The flux on the centerline of a sampling orifice with radius r_1 at the distance $x \gg r_1$ in the free molecular flow conditions is:[56]

$$F(x) = \frac{1}{4} n_0 \nu_{\text{average}} \left(\frac{r_1}{x} \right)^2, \qquad (A2)$$

where $\nu_{\text{average}} = (8 \, kT / \pi m)^{0.5}$ is an average velocity. All the beam species on the centerline of the orifice move approximately in the same direction giving $F(x) = n^{\text{beam}}(x) \nu_{\text{average}}$. The beam number density at a distance $x(x \gg r_1)$ is then given by:

$$n^{\text{beam}}(x) = \frac{1}{4} n_0 \left(\frac{r_1}{x} \right)^2. \qquad (A3)$$

The factor of $\frac{1}{4}$ is missing in the original expression given by Coburn and Kay[57] as well as in the article of Singh *et al.*[3] However, since the expression (A3) is used for both calibration gas and species of interest, the factor of $\frac{1}{4}$ cancels and does not influence the obtained density value.

The beam species enter the third stage with velocity ν_{average} and after passing the ionizer they finally collide with the QMS parts and contribute to the background pressure in the third stage. This additional background is not included in the residual background as calculated in Eq. (A1) and can be expressed as:

$$n_{\text{add}}^{\text{background}} = \frac{A_{\text{beam},3} F(x_3)}{S_3} = A_{\text{beam},3} \cdot n^{\text{beam}}(x_3) \cdot \nu_{\text{average}} \frac{1}{S_3}, \qquad (A4)$$

where x_3 is the distance from the sampling orifice to the third orifice, $n^{\text{beam}}(x_3)$ is the beam density at the third orifice, S_3 the effective pumping speed in the third stage, and $A_{\text{beam},3}$ is the beam cross section area at the distance x_3 determined by the beam solid angle formed either by the second orifice at distance x_2 or the third orifice at distance x_3 from the sampling orifice. It should be noticed that the value of this additional background does not depend on the pumping speeds in the first and second stages. The beam-to-background calculation can now be expressed using both residual and addi-

tional backgrounds. One more correction should be taken into account in the case where the beam does not completely fill the ionizer volume. Then the final beam-to-background ratio depends also on the ratio of the beam volume in the ionizer (V_{beam}) to the ionizer effective volume ($V_{ionizer}$). Then we obtain for the beam-to-background ratio:

$$R = \frac{V_{beam}}{V_{ionizer}} \frac{n^{beam}}{n_{add}^{background} + n_3^{background}}, \tag{A5}$$

with

$$V_{beam} = A_{beam,ion} l_{ionizer}, \tag{A6}$$

$$V_{ionizer} = A_{ionizer} l_{ionizer}, \tag{A7}$$

where $A_{ionizer}$ and $I_{ionizer}$ are the ionizer cross section area and length, respectively, and $A_{beam,ion}$ is the beam cross section area in the ionizer. Since we observed much higher background pressure when the chopper is open, first the situation with the negligible residual background $n_3^{background}$ is considered. It is just the opposite extreme situation than the one treated by Singh *et al.*[3] Combining Eqs. (A3)–(A7) and using the relation:

$$\frac{A_{beam,ion}}{A_{beam,3}} = \left(\frac{x_{ion}}{x_3}\right)^2, \tag{A8}$$

where x_{ion} is the sampling orifice-ionizer distance, one can derive:

$$R_{onlybeam} = \frac{S_3}{\nu_{average} A_{ionizer}}. \tag{A9}$$

This is the highest possible "theoretical" beam-to-background ratio, which can be achieved with a given setup. The $\nu_{average}$ is determined by the gas temperature and $A_{ionizer}$ is determined by the available ionizer design and hence the most important parameter influencing the final beam-to-background ratio is the effective pumping speed in the last stage. When the beam diameter is smaller than ionizer diameter, the beam-to-background ratio calculated in Eq. (A9) does not depend on the ionizer distance from the first orifice. However, the ion extraction efficiency of the real ionizer will be maximal on its axis and will decrease towards the ionizer sides. Therefore, in the real situation, the net beam signal and beam-to-background ratio will always decrease if the first orifice-ionizer distance is increasing.

When the residual background is also included, the beam-to-background ratio gets even smaller. Calculation made for the C_2H_2 gas predicts a 14 times pressure increase in the last stage between chopper blocking and chopper open positions and a real beam-to-background ratio with chopper open of 0.68. Experimental results for 1 Pa of C_2H_2 in the reactor (effusive sampling through the first orifice) gives a 9.5 times pressure increase and beam-to-background ratio of 0.86, reasonably close to the predicted values. The pressure under our typical deposition conditions is 29 Pa, which means that the first orifice diameter is bigger than the mean free path, and the assumption of the molecular flow cannot be used. The transition flow throughput through the orifice is bigger than

the molecular flow throughput,[58] resulting in higher residual background density than calculated on the basis of Eq. (A1). The beam density will also be influenced and can differ from the expected value calculated in Eq. (A3). However, Eq. (A9) can still be used to characterize the theoretical beam-to-background ratio because it is neither dependent on the beam density nor on the beam flux into the third stage.

[1] S. Agarwal, G. W. W. Quax, M. C. M. van de Sanden, D. Maroudas, and E. S. Aydil, J. Vac. Sci. Technol. A **22**, 71 (2004).
[2] P. Kae-Nune, J. Perrin, J. Guillon, and J. Jolly, Plasma Sources Sci. Technol. **4**, 250 (1995).
[3] H. Singh, J. W. Coburn, and D. B. Graves, J. Vac. Sci. Technol. A **17**, 2447 (1999).
[4] H. Singh, J. W. Coburn, and D. B. Graves, J. Vac. Sci. Technol. A **18**, 299 (2000).
[5] V. M. Donnelly, J. Appl. Phys. **79**, 9353 (1996).
[6] S. Agarwal, B. Hoex, M. C. M. van de Sanden, D. Maroudas, and E. S. Aydil, Appl. Phys. Lett. **83**, 4918 (2003).
[7] W. L. Hsu and D. M. Tung, Rev. Sci. Instrum. **63**, 4138 (1992).
[8] H. Wang and M. Frenklach, Combust. Flame **110**, 173 (1997).
[9] C. S. McEnally, L. D. Pfefferle, A. G. Robinson, and T. S. Zwier, Combust. Flame **123**, 344 (2000).
[10] M. Frenklach and H. Wang, Phys. Rev. B **43**, 1520 (1991).
[11] A. von Keudell, T. Schwarz-Selinger, W. Jacob, and A. Stevens, J. Nucl. Mater. **290–293**, 231 (2001).
[12] P. M. Woods, T. J. Millar, E. Herbst, and A. A. Zijlstra, Astron. Astrophys. **402**, 189 (2003).
[13] C. N. Keller, V. G. Anicich, and T. E. Cravens, Planet. Space Sci. **46**, 1157 (1998).
[14] J. Robertson, Mater. Sci. Eng., R. **R37**, 129 (2002).
[15] J. W. A. M. Gielen, P. R. M. Kleuskens, M. C. M. van de Sanden, L. J. van IJzendoorn, D. C. Schram, E. H. A. Dekempeneer, and J. Meneve, J. Appl. Phys. **80**, 5986 (1996).
[16] M. C. M. van de Sanden, R. J. Severens, J. W. A. M. Gielen, R. M. J. Paffen, and D. C. Schram, Plasma Sources Sci. Technol. **5**, 268 (1996).
[17] R. Engeln, K. G. Y. Letourneur, M. G. H. Boogaarts, M. C. M. van de Sanden, and D. C. Schram, Chem. Phys. Lett. **310**, 405 (1999).
[18] J. Benedikt, R. V. Woen, S. L. M. van Mensfoort, V. Perina, J. Hong, and M. C. M. van de Sanden, Diamond Relat. Mater. **12**, 90 (2003).
[19] J. Benedikt, M. Wisse, R. V. Woen, R. Engeln, and M. C. M. van de Sanden, J. Appl. Phys. **94**, 6932 (2003).
[20] W. M. M. Kessels, M. C. M. van de Sanden, and D. C. Schram, J. Vac. Sci. Technol. A **18**, 2153 (2000).
[21] W. M. M. Kessels, M. C. M. van de Sanden, and D. C. Schram, Appl. Phys. Lett. **72**, 2397 (1998).
[22] W. M. M. Kessels, C. M. Leewis, M. C. M. van de Sanden, and D. C. Schram, J. Appl. Phys. **86**, 4029 (1999).
[23] W. M. M. Kessels, A. Leroux, M. G. H. Boogaarts, J. P. M. Hoefnagels, M. C. M. van de Sanden, and D. C. Schram, J. Vac. Sci. Technol. A **19**, 467 (2001).
[24] W. M. M. Kessels, F. J. H. van Assche, J. Hong, D. C. Schram, and M. C. M. van de Sanden, J. Vac. Sci. Technol. A **22**, 96 (2004).
[25] J. W. A. M. Gielen, M. C. M. van de Sanden, P. R. M. Kleuskens, and D. C. Schram, Plasma Sources Sci. Technol. **5**, 492 (1996).
[26] C. Leewis (unpublished).
[27] R. Rejoub, B. G. Lindsay, and R. F. Stebbings, Phys. Rev. A **65**, 042713 (2002).
[28] B. G. Lindsay and M. A. Mangan, in *Landolt-Börnstein*, I/17/C, edited by Y. Itikawa.
[29] V. Tarnovsky, A. Leven, H. Deutsch, and K. Becker, J. Phys. B **29**, 139 (1996).
[30] K. L. Bell, H. B. Gilbody, J. G. Hughes, A. E. Kingston, and F. J. Smith, J. Phys. Chem. Ref. Data **12**, 891 (1983).
[31] B. L. Schram, M. J. van der Wiel, F. J. de Heer, and H. R. Moustafa, J. Chem. Phys. **44**, 49 (1966).
[32] A. Berman, *Vacuum Engineering Calculations, Formulas, and Solved Exercises* (Academic, New York, 1992).
[33] P. P. Wegener, *Molecular Beams and Low Density Gasdynamics* (Marcel Dekker, New York, 1974).

[34]E. L. Knuth, Combust. Flame **103**, 171 (1995).

[35]*Atomic and Molecular Beam Methods*, edited by G. Scoles (Oxford University Press, Oxford, 1988), Vol. I.

[36]J. W. A. M. Gielen, W. M. M. Kessels, M. C. M. van de Sanden, and D. C. Schram, J. Appl. Phys. **82**, 2643 (1997).

[37]A. de Graaf, M. F. A. M. van Hest, M. C. M. van de Sanden, K. G. Y. Letourneur, and D. C. Schram, Appl. Phys. Lett. **74**, 2927 (1999).

[38]A. M. Derkatch, A. Al-Khalili, L. Vikor, A. Neau, W. Shi, H. Danared, M. Ugglas, and M. Larsson, J. Phys. B **32**, 3391 (1991).

[39]M. C. M. van de Sanden, J. M. de Regt, and D. C. Schram, Plasma Sources Sci. Technol. **3**, 511 (1994).

[40]*NIST Chemistry WebBook*, edited by P. J. Linstrom and W. G. Mallard, NIST Standard Reference Database Number 69 (National Institute of Standards and Technology, Gaithersburg MD) ⟨http://webbook.nist.gov⟩.

[41]P. J. Chantry, J. Appl. Phys. **62**, 1141 (1987).

[42]J. Perrin, M. Shiratani, P. Kae-Kune, H. Videlot, J. Jolly, and J. Guillon, J. Vac. Sci. Technol. A **16**, 278 (1998).

[43]V. Philipps, E. Vietzke, and K. Flaskamp, Surf. Sci. **178**, 806 (1986).

[44]M. Stano, S. Matejcik, J. D. Skalny, and T. D. Märk, J. Phys. B **36**, 261 (2003).

[45]M. Rubio, J. Starling, A. Bernhardsson, R. Lindh, and B. O. Roos, Theor. Chem. Acc. **105**, 15 (2000).

[46]H. Clauberg, D. W. Minsek, and P. Chen, J. Am. Chem. Soc. **114**, 99 (1992).

[47]W. Boullart, K. Devriend, R. Borms, and J. Peeters, J. Phys. Chem. **100**, 998 (1996).

[48]R. T. Meyer, A. W. Lynch, and J. M. Freese, J. Phys. Chem. **77**, 1083 (1973).

[49]A. M. Mebel and R. I. Kaiser, Chem. Phys. Lett. **360**, 139 (2002) and references therein.

[50]Yu. A. Mankelevich, N. V. Suetin, M. N. R. Ashfold, W. E. Boxford, A. J. Orr-Ewing, J. A. Smith, and J. B. Wills, Diamond Relat. Mater. **12**, 383 (2003).

[51]R. Ramanathan, J. A. Zimmerman, and J. R. Eyler, J. Chem. Phys. **98**, 7838 (1993).

[52]J. R. Wyatt and F. E. Stafford, J. Phys. Chem. **76**, 1913 (1972).

[53]R. I. Kaiser, C. Ochsenfeld, M. Head-Gordon, Y. T. Lee, and A. G. Suits, J. Chem. Phys. **106**, 1729 (1997).

[54]J. Benedikt, D. J. Eijkman, W. Vandamme, S. Agarwal, and M. C. M. van de Sanden, Chem. Phys. Lett. **402**, 37 (2005).

[55]J. Benedikt, D. C. Schram, and M. C. M. van de Sanden (unpublished).

[56]R. E. Stickney, R. F. Keating, S. Yamamoto, and W. J. Hastings, J. Vac. Sci. Technol. **4**, 10 (1967).

[57]J. W. Coburn and E. Kay, J. Vac. Sci. Technol. **8**, 738 (1971).

[58]S. F. DeMuth, J. S. Watson, J. Vac. Sci. Technol. A **4**, 344 (1986).